Reprinted from

ELSEVIER SEQUOIA S.A., LAUSANNE

Thin Solid Films, *212* (1992) 206–215

First-order Raman scattering in homoepitaxial chemical vapor deposited diamond at elevated temperatures

H. Herchen and M. A. Cappelli
High Temperature Gasdynamics Laboratory, Stanford University, Stanford, CA 94305-3032 (USA)
M. I. Landstrass, M. A. Plano and M. D. Moyer
Crystallume, Inc., 125 Constitution Drive, Menlo Park, CA 94025 (USA)

(Received August 5, 1991)

Abstract

The polarization discriminated first-order Raman spectrum in homoepitaxial chemical vapor deposited diamond was measured for the temperature range 300–1200 K. The dependences of Raman shift and width on temperature for natural type IIa diamond over the temperature range 300–2000 K are also given for comparison. Both the Stokes and anti-Stokes components were analyzed for their intensity, Raman shift, and width variation with temperature. The polarization of the Raman signal from the synthetic-diamond–natural-diamond laminate at elevated temperatures was found to be the same as that at room temperature. The observed Raman shift, however, indicated the presence of internal stress. We attribute this homogeneous stress to a lattice mismatch which we speculate arises from hydrogen incorporation during growth. Following extended exposure to high temperatures *in vacuo*, the position of the first-order Raman peak at room temperature was found to relax to that measured for natural diamond.

1. Introduction

Growth of thin diamond films by chemical vapor deposition (CVD) at relatively low pressures and temperatures has become a promising new technology, with applications ranging from the engineering of wear-resistant coatings to high speed microelectronic devices [1–5]. The advantageous use of such films, especially at elevated temperatures, presupposes that their properties are similar to or better than those of natural diamond. One useful method of comparing the quality of CVD diamond to that of natural diamond makes use of the distinct Raman scattering signature that discriminates diamond from other allotropes of carbon. In fact, Raman scattering has now been established as one of the standard characterization techniques for CVD diamond.

The lattice dynamics that give rise to the Raman effect also determine the thermal properties such as the specific heat and thermal conductivity [6]. *In situ* monitoring of the growth of plasma-enhanced CVD diamond by Raman spectroscopy may lead to better process control and hence to significant improvement in yields. As an *in situ* monitor, such measurements will have to be performed at elevated temperatures, typically 1100 K, which appears to be the optimal temperature for high quality diamond growth. The high temperature first-order Raman spectrum of diamond needs to be further studied before it is used as an appropriate standard. This requires accurate measurements of the Raman shift, spectral width, overall scattering yield and polarization characteristics at elevated temperatures in natural diamond. Any one of these features, acquired *in situ* or *ex situ*, can be useful in comparing the quality of CVD diamond with that of natural diamond. In this paper, we describe and compare *ex situ* measurements of the first-order Raman spectra of natural and homoepitaxial CVD diamond at elevated temperatures.

It is well known that stress, in the absence of temperature changes, induces a shift in the Raman spectrum [7, 8]. In CVD diamond grown on foreign substrates, this stress may arise from a lattice mismatch between the deposited diamond and the substrate, or it may arise from a difference in their thermal expansion coefficients. Residual stress inferred from differences in the position of the Raman peak in CVD diamond when compared with that of natural diamond [9] may be indicative of structural differences between the properties of synthetic CVD diamond and those of natural diamond. At the microscopic level, the stress is associated with changes in the average atomic spacing which in turn influences the normal modes of vibration through anharmonic contributions to the interaction potential.

At constant pressure, changes in temperature are also known to alter the Raman spectrum of diamond [10–12]. The dominant mechanisms responsible for shifting

0040-6090/92/$5.00

and broadening the first-order Raman spectrum in diamond are (i) thermal expansion, (ii) optical phonon–phonon coupling, and (iii) the decay of optical phonons to two acoustical phonons of equal and opposite momentum. All three mechanisms are attributed to anharmonic interactions. Elevated temperatures are accompanied by thermal expansion and hence changes in average atomic separation. Further, the increase in temperature excites higher vibrational states having greater amplitude which experience different anharmonic contributions and are therefore shifted in frequency. Finally, anharmonic interactions can lead to the decay of single zone-center optical phonons into two zone-boundary acoustical phonons with a concomitant reduction in the optical phonon lifetime [12]. The latter interaction manifests itself primarily as a broadening and possible depolarization of the first-order Raman spectrum.

The temperature dependence of the first-order Raman line in diamond up to approximately 1000 K has been measured previously by a number of investigators [13–18]. Herchen and Cappelli [19] and Zouboulis and Grimsditch [20] have recently performed detailed measurements of both the Raman shift and broadening of the first-order Raman spectrum at temperatures as high as 1900 K. We report here on an extension of our previous work [19] to somewhat higher temperatures in natural diamond, and in addition describe a detailed study of the polarization characteristics of the scattered light at elevated temperatures. These data form the basis for a comparison with those obtained from homoepitaxial diamond grown by microwave CVD.

The polarization of Raman scattered light is dependent on scattering geometry and crystal orientation as well as on the crystal structure [21]. For linearly polarized excitation photons and the forward scattering geometry of the present experiments, the Raman scattered light will be linearly polarized for certain orientations of the crystal. Polycrystalline materials, with their random crystallite orientation, will not exhibit polarization of the Raman signal if the excitation volume is much larger than the average crystallite size. Hence measurements of the polarization properties can be used to probe the crystal orientation and structure, as has been done *ex situ* for thin CVD diamond film at room temperature [22]. To utilize fully polarization discriminated Raman scattering as an *in situ* characterization during epitaxial growth, depolarization associated with two-phonon decay at elevated temperatures must be evaluated.

For single diamond crystals, with forward scattering geometry and linearly polarized light incident normal to the (111) surface, the Raman scattered light intensity will be independent of analyzer angle. When the crystal orientation is modified to have the (100) surface normal to the incident light, the Raman signal will be linearly polarized, with a polarization angle that depends on the relative angle between the polarization of the incident light and the principal axes of the crystal.

The intensity S of Raman scattered light as a function of polarization can be found from [21]

$$S \propto \left[\sum_{\rho,\,\sigma = x,\,y,\,z} \mathbf{e}_i^{\sigma} R_{\sigma\rho} \mathbf{e}_s^{\rho} \right]^2 \tag{1}$$

where $\mathbf{e}_i$ and $\mathbf{e}_s$ are the unit vectors describing the direction of polarization of the incident and scattered light respectively. For the Raman active F mode of diamond,

$$R_{\sigma\rho} = \begin{bmatrix} 0 & 0 & 0 \\ 0 & 0 & d \\ 0 & d & 0 \end{bmatrix}, \begin{bmatrix} 0 & 0 & d \\ 0 & 0 & 0 \\ d & 0 & 0 \end{bmatrix}, \begin{bmatrix} 0 & d & 0 \\ d & 0 & 0 \\ 0 & 0 & 0 \end{bmatrix} \tag{2}$$

for the x, y, and z directions respectively, associated with the principal axes of the diamond crystal.

The ratio of the intensities of the Stokes and anti-Stokes components [23]

$$\frac{I_{St}}{I_{a-St}} = \left(\frac{\nu_l - \nu_s}{\nu_l + \nu_s} \right)^4 \exp(h\nu_s / kT) \tag{3}$$

can provide a direct measure of the sample temperature. Here ν_s is the phonon frequency, ν_l is the line center frequency of the laser excitation source, T is the sample temperature, and h and k are the Planck and Boltzmann constants. This equation has been used as an unambiguous measure of sample temperature in a range of materials by a number of investigators [17, 24–26]. The sample must be optically thin at the Stokes and anti-Stokes wavelengths if the equation is to be used without modification.

2. Experimental details

Three (100) oriented diamond samples were used in this study. Two were natural type IIa diamond plates with dimensions $2 \times 2 \times 0.25\ \text{mm}^3$. The third sample consisted of a homoepitaxial layer on natural type IIa diamond described in more detail below.

Diamond deposition to form this third sample was performed by microwave plasma-assisted CVD using mixtures of methane in hydrogen with added oxygen-containing compounds. The substrate temperature, deposition pressure and microwave power were nominally 1100 K, 60 Torr, and 2 kW respectively. Natural (100) oriented diamond substrates of dimensions $1 \times 1 \times 0.1\ \text{mm}^3$ were initially etched in a hydrogen plasma and subsequently analyzed prior to growth to reveal a relatively high density of stacking faults (typically $10^5\ \text{cm}^{-2}$). As a result of the relatively high level of

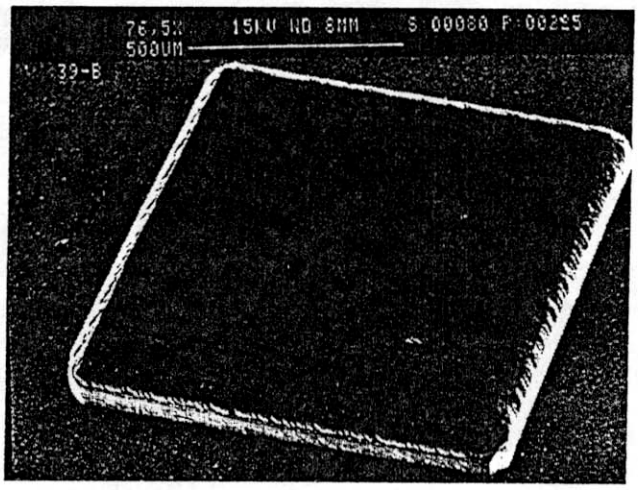

Fig.1. Scanning electron micrograph of 120 μm diamond single-crystal epitaxial layer deposited homoepitaxially onto a (100) type IIa diamond with dimensions $1 \times 1 \times 0.1$ mm^3. The diamond epitaxial layer can be distinguished from the substrate by the rough edges present only on the grown layer.

defects in the natural diamond substrates, deposition conditions ordinarily used for polycrystalline diamond film synthesis with only methane and hydrogen gas mixtures were found to yield homoepitaxial films with a high density of polycrystalline inclusions. This interaction of stacking faults within the substrate and the CVD diamond process is not well understood. It was found that with the addition of oxygen-containing precursors, the polycrystalline inclusions could be minimized. The homoepitaxial layers grown in such a manner were found to have a low macroscopic defect density as revealed by the measurements of polarization-sensitive Raman scattering described below.

The homoepitaxial single-crystal layer tested and reported on here was approximately 120 μm thick. Shown in Fig. 1 is a scanning electron micrograph of the 120 μm epitaxial layer on the 100 μm thick natural diamond substrate. As can be seen from the micrograph, this layer is very smooth except at the edges. The epitaxial layer can be distinguished from the substrate by these rough edges. A 120 μm thick polycrystalline layer surrounds what we shall call the synthetic-diamond–natural-diamond laminate. This polycrystalline diamond nucleated on an underlying silicon wafer was chemically etched prior to Raman analysis to leave behind a free-standing 1×1 cm^2 polycrystalline diamond wafer surrounding the synthetic-diamond–natural-diamond laminate.

Raman spectra were obtained by exciting the diamond samples with one of two lasers, an argon ion laser (Lexel Model 85) mechanically chopped at 2 kHz or a Spectra Physics Nd/YLF pulsed laser (Spectra-Physics model 7960-L3, Spectra-Physics, Mountain View, CA). The argon ion 457.94 nm output was selected since the intrinsic black body emission is less at this wavelength than at 514.5 nm, the latter wavelength being commonly used in micro-Raman analysis. The Nd/YLF laser output was frequency doubled to 523.4 nm and had a pulse width of 7 ns. A schematic diagram of the facility is given in Fig. 2. In all cases, the incident laser direction was along the [100] or x axis, *i.e.* normal to the (100) face of the diamond samples. The laser was linearly polarized along the [010] or y axis of the sample. The vertical to horizontal polarization ratio did not change appreciably on reflection from the front surface mirror. For the Raman shift and width data, the forward scattered light was unanalyzed for its polarization. For the measurements of the polarization of the scattered light, a rotatable sheet polarizer was placed before the monochromator entrance slit. A tungsten filament lamp in conjunction with a sheet polarizer was used to determine the relative system response for both vertically and horizontally polarized light at all relevant wavelengths. All intensities are corrected for system throughput and given in power units rather than photon count rates. Additional details are given elsewhere [19].

The diamond samples were sandwiched between two electrically heated tungsten ribbons and were free to expand thermally, as shown in the inset to Fig. 2. With this geometry, the natural diamond was nearly completely surrounded by the tungsten filaments, and would come to thermal equilibrium with the filament through conduction and radiant energy exchange. The tungsten temperature was measured by optical pyrometry, with a Pyro Micro Model 85 disappearing filament pyrometer, making appropriate correction for the tungsten emissivity [27]. In order to verify that the natural diamond was in thermal equilibrium with the tungsten filaments, its temperature was independently determined from the Stokes-to-anti-Stokes component intensity ratios, as discussed in Section 3. As previously described, the synthetic-diamond–natural-diamond laminate consisted of a homoepitaxially grown region 1 mm^2 surrounded by a polycrystalline region about 1 cm^2. This larger sample radiated sufficiently at higher temperatures so that it was at a somewhat lower temperature than the tungsten heaters. At elevated temperatures, this sample's temperature was determined solely from the Stokes-to-anti-Stokes intensity ratio.

The diamond samples and filament heaters were placed within a specially designed high vacuum chamber with optical access. The chamber pressure during runs was maintained below 10^{-5} Torr, thereby preventing contamination due to oxidation or premature graphitization of the diamond sample. For experiments where the argon ion laser was used, potential contamination was assessed by monitoring the transmission of

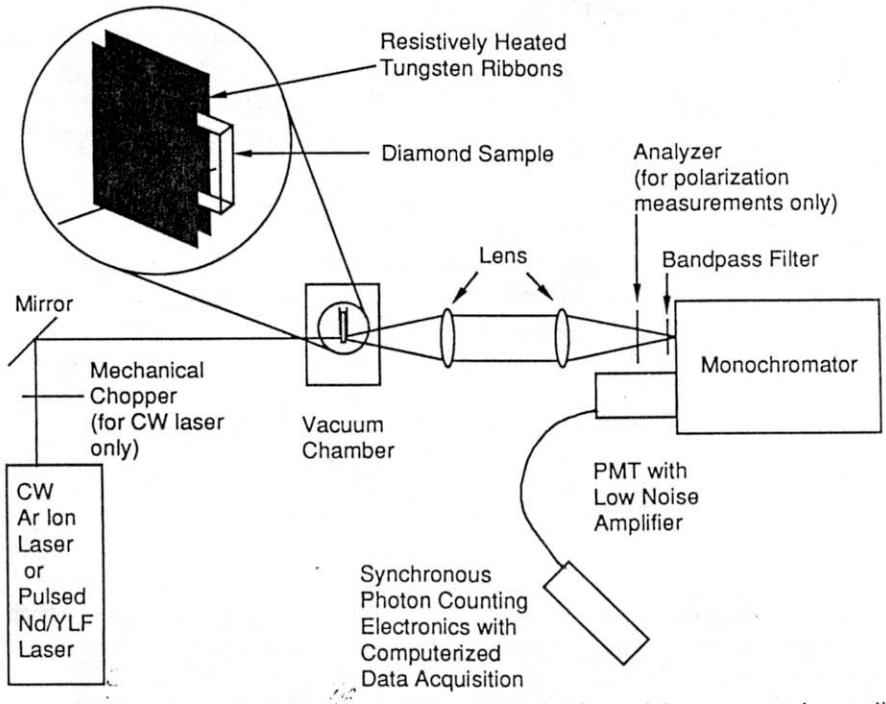

Fig. 2. Schematic diagram of the experimental set-up for forward Raman scattering studies of natural and synthetic diamond at high temperature. The inset illustrates the mechanism employed to heat, hold, and interrogate the sample. The argon ion laser and the mechanical chopper were replaced by a Spectra-Physics pulsed Nd/YLF laser for some measurements, as indicated in the text.

nearby argon ion plasma emission lines originating from the laser discharge tube. These lines also served as accurate and absolute wavelength references. With the Raman scattering components being excited by the 457.94 nm laser line, the nearby $Ar^+ 4s\ ^2P \rightarrow 4p\ ^2D^o$ line at 487.986 nm lay reasonably close to the Stokes component, and $4s''\ ^2S \rightarrow 5p\ ^2P^0$ and $3d\ ^2F \rightarrow 4p'\ ^2D^0$ unresolved spectral lines at 430.924 nm and 430.909 nm were sufficiently close to the anti-Stokes component. These emission lines also served as convenient references for the instrument contribution to the Raman line broadening, as they were predominantly instrument broadened under conditions expected within the laser discharge cavity. For experiments using Nd/YLF pulsed laser excitation, no absolute calibration lines were used simultaneously with each Raman scan. However, it was found that the monochromator wavelength could be repeatably set to better than 0.02 nm. The absolute wavelength reading for this case was found before the experiment using a mercury emission lamp.

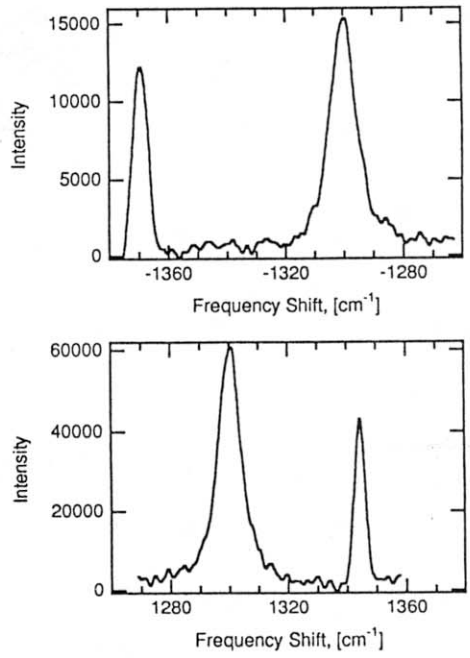

Fig. 3. Representative anti-Stokes (top) and Stokes Raman spectra with argon ion emission calibration lines. The natural diamond temperature was 1470 K.

3. Results and discussion

Typical Stokes and anti-Stokes first-order Raman spectra of natural type IIa diamond at a temperature of 1470 ± 40 K are shown in Fig. 3. The Raman spectra observed here for the synthetic-diamond–natural-diamond laminate are similar. The nearby argon plasma emission lines appear at 1345 cm^{-1} and 1370 cm^{-1} shifts. As expected, the observed Stokes and anti-Stokes shifts are equal and approximately 1300 cm^{-1}, and considerably less than the room temperature shift of 1332.5 cm^{-1}

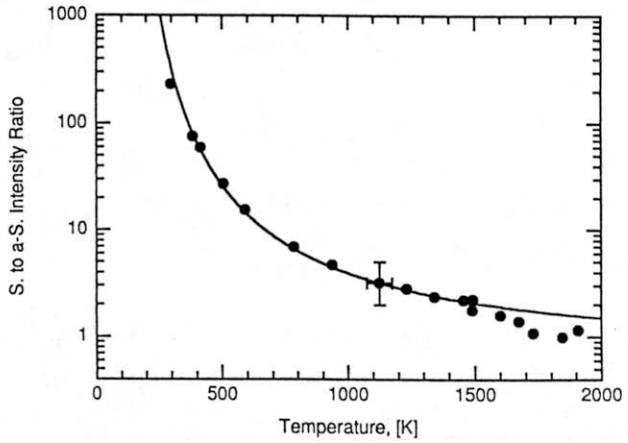

Fig. 4. Comparison of measured and theoretical Stokes-to-anti-Stokes intensity ratios for the frequency doubled Nd/YLF laser excitation at 523.4 nm.

for unstressed natural diamond. In addition, the lines are significantly broader than the nearby argon plasma reference lines.

The variation of the computed Stokes-to-anti-Stokes ratio with temperature for the Nd/YLF laser at 523.4 nm is shown in Fig. 4 (solid curve), along with the experimentally derived data for the natural diamond. The close agreement between the measured and theoretical temperature dependence suggests that the natural diamond sample is optically thin to the laser, Stokes, and anti-Stokes radiation. This is as expected for diamond, and no corrections have been made for self absorption. One can reasonably conclude that the natural diamond sample temperature was not appreciably different from that of the tungsten heaters. Although the curves are not shown here, the synthetic-diamond–natural-diamond laminate showed significant differences between the tungsten and actual temperature, as determined through the Stokes-to-anti-Stokes ratio. The difference ranged from zero at room temperature to about 250 K at 1200 K diamond temperature. This was as expected, since the sample had a much larger radiating area than the natural diamond sample. Owing to this temperature difference, the results for the synthetic diamond are plotted using the Stokes-to-anti-Stokes intensity ratio based temperature.

3.1. First-order Raman shift

Variation in the observed Raman shift with temperature for both the Stokes and anti-Stokes components of natural diamond is shown in Fig. 5. This figure is a compilation of earlier data [13, 15, 16, 19], and of the recent data of Zouboulis and Grimsditch [20]. This figure includes our new Nd/YLF laser-derived data providing a further increase in the temperature range to reach 2000 K. These data were obtained from the second natural type IIa diamond sample, and are shown in

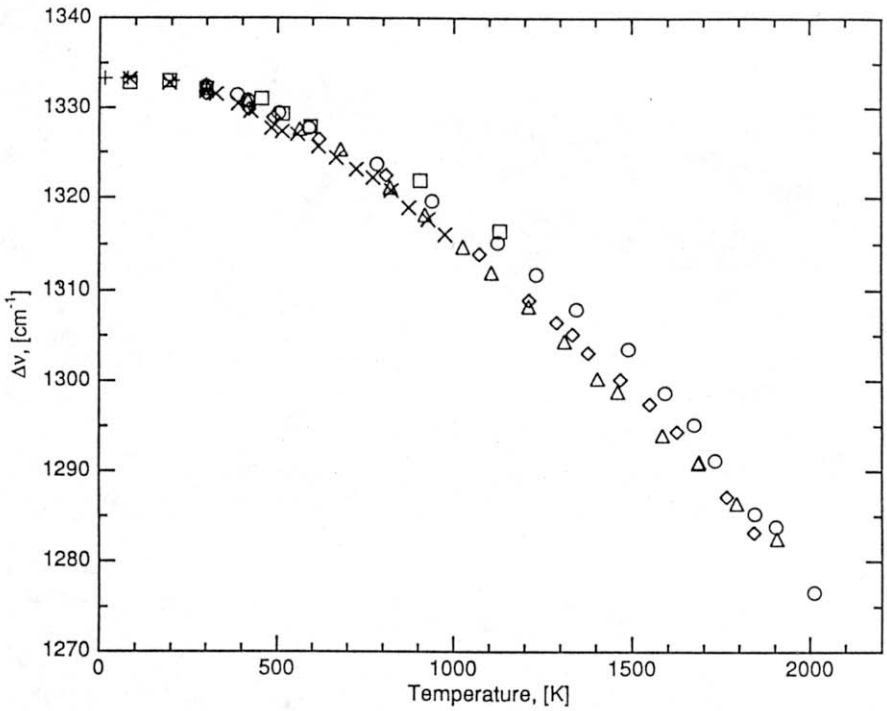

Fig. 5. Variation with temperature of the first-order Raman shift in natural diamond. The data are represented as circles for our present results with the Nd/YLF laser, and squares, crosses, pluses, and triangles for refs. 13, 15, 16, and 20 respectively. The data represented by the diamond shaped symbols are from our earlier results using an argon ion laser [19].

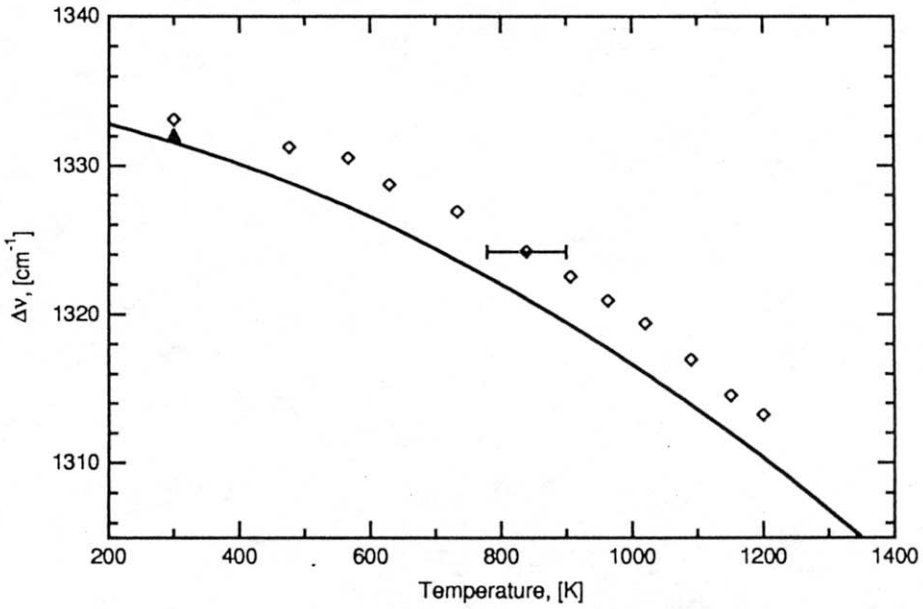

Fig. 6 The open symbols are the experimentally observed variation with temperature in the first-order Raman shift for the synthetic-diamond–natural-diamond laminate. The solid triangle is the observed room temperature shift of this sample after annealing. The solid line represents a fit to the results for natural diamond.

the open circles of Fig. 5. The uncertainties in the frequency shift are $\pm 0.3\ \mathrm{cm}^{-1}$ for the argon ion laser and $\pm 1\ \mathrm{cm}^{-1}$ for the Nd/YLF laser. The error in the temperature arises primarily from the uncertainties in the use of the disappearing filament pyrometer for measuring the tungsten temperature. The compiled experimental data are well represented by the curve

$$\Delta\nu = a_1 T^2 + a_2 T + a_3 \tag{4}$$

with coefficients $-1.124 \times 10^{-5}\ \mathrm{cm}^{-1}\ \mathrm{K}^{-2}$, $-6.71 \times 10^{-3}\ \mathrm{cm}^{-1}\ \mathrm{K}^{-1}$, and $1334.5\ \mathrm{cm}^{-1}$ respectively, having standard deviations of 1.4×10^{-7}, 2.8×10^{-4}, and 0.12 respectively. The coefficients for this fit are a few per cent different from those found earlier [19].

The variation with temperature in the observed Raman shift for the synthetic-diamond–natural-diamond laminate is shown in Fig. 6. The temperatures are obtained from the Stokes-to-anti-Stokes intensity ratio. It should be kept in mind that this sample comprises CVD diamond that was grown on an approximately equal thickness of natural diamond. This results in approximately equal percentages of natural and synthetic diamond in the imaged volume. The solid line in this figure is the fit to the data on the Raman shift of natural diamond found earlier, eqn. (4). The argon ion laser at 457.94 nm was used as the excitation source for the study of this synthetic-diamond–natural-diamond laminate. The error in the temperature arises primarily from the uncertainties in the integrated intensities of the Stokes and anti-Stokes Raman spectra. It is clear from Fig. 6 that the synthetic-diamond–natural-diamond laminate is under compressive stress, resulting in a difference of $2–3\ \mathrm{cm}^{-1}$ in the shift, even at room temperature, compared with that of natural diamond at the same temperature. This is true for the full range of temperatures observed. It is noted, however, that these data were accumulated over many hours in order of increasing temperature. Following acquisition of the data at 1200 K, additional scans at room temperature revealed a relaxation of the sample and a Raman shift essentially equal to that of natural diamond. In essence, the high temperature studies resulted in a relatively extended thermal anneal. Figure 7 shows the room temperature Raman spectrum as deposited and following a relatively long exposure of many hours to high temperatures and high vacuum. The centers of the shifts are at $1333.6\ \mathrm{cm}^{-1}$ prior to heating and $1332.1\ \mathrm{cm}^{-1}$ after heating and prolonged exposure to vacuum. This change in the shift is significant. There is, however, no experimentally significant difference between the room temperature full widths at half-maximum (FWHM) intensities of these two spectra.

We speculate here that hydrogen incorporation during growth was responsible for the homogeneous stress observed over the wide temperature range. Gradual desorption over time at elevated temperatures can account for the relaxation in the room temperature spectrum measured at the end of the experiment. Hydrogen desorption and subsequent reconstruction has been found by others [28]. Annealing of point defects in the synthetic diamond could also be a factor in the reduction of this stress.

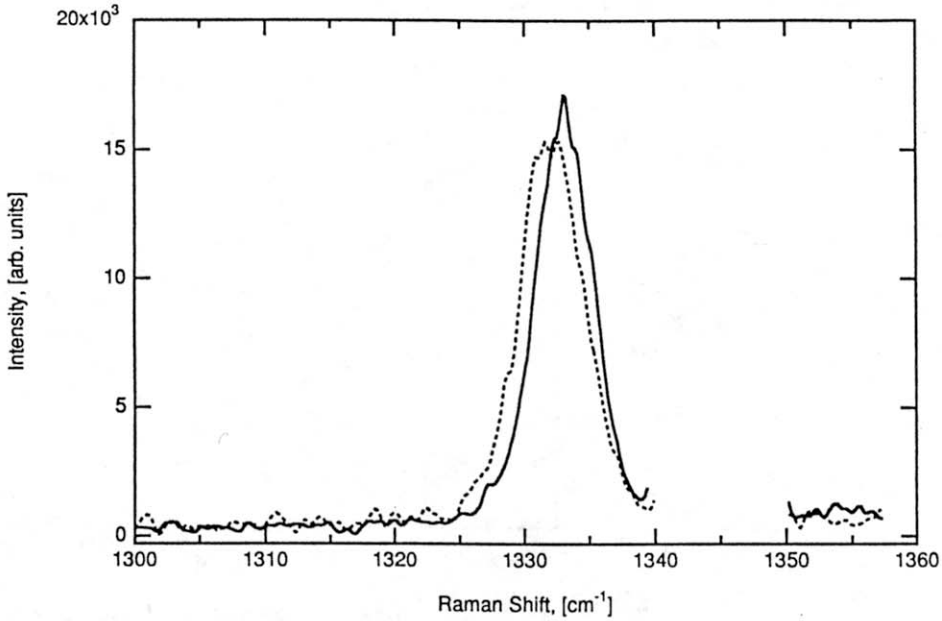

Fig. 7. Comparison of the room temperature first-order Raman spectra for the synthetic-diamond–natural-diamond laminate before (——) and after (– – –) heating. The argon ion laser plasma calibration lines have been removed for clarity.

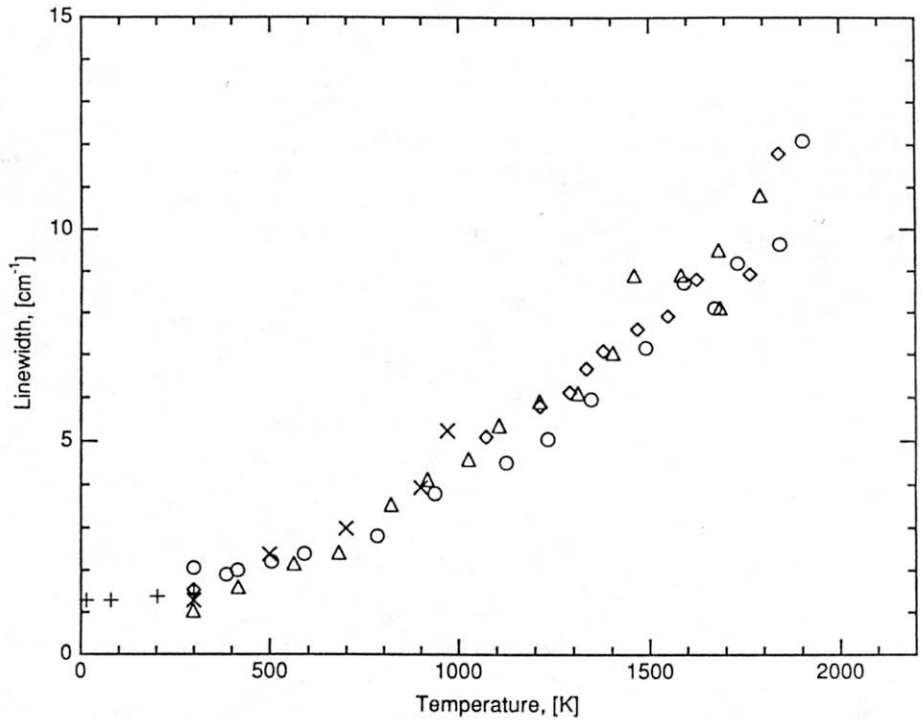

Fig. 8 Variation with temperature of the FWHM of the first-order Raman spectrum in natural diamond. The data are represented as circles for our present results with Nd/YLF laser, and crosses, pluses, and triangles for refs. 15, 16, and 20 respectively. The data represented by the diamond shaped symbols are from our earlier results using an argon ion laser [19].

3.2. *First-order Raman width*

The variation with temperature in the FWHM intensity for natural diamond is shown in Fig. 8. Also shown for comparison are earlier experimental data [15, 16, 19] and the recent data of Zouboulis and Grimsditch [20]. Our spectral lineshapes were found to be well represented by a Voigt function. The Lorentzian Raman scattered contribution to the lineshape was found by deconvolving the Gaussian instrument broadening from the actual spectra. The instrument broadening

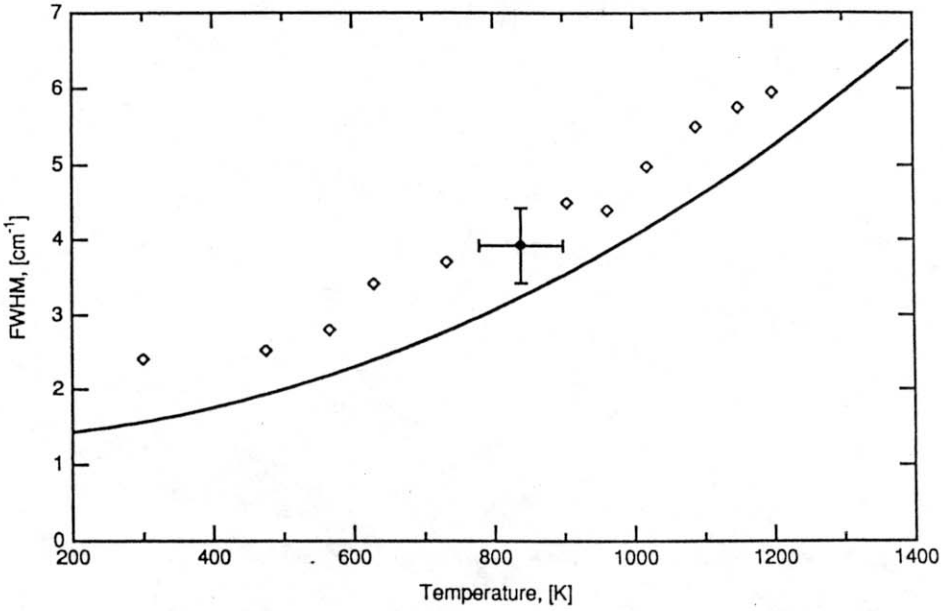

Fig. 9. Experimentally observed variation of the FWHM of the first-order Raman spectrum in the synthetic-diamond–natural-diamond laminate with temperature. The solid line represents a fit to the results for natural diamond.

contribution to the measured spectra was Gaussian in shape, with FWHM of 3.7 cm^{-1} and 4.7 cm^{-1} for the Stokes and anti-Stokes lines respectively. The data given by Zouboulis and Grimsditch were not corrected for instrument broadening. This correction was performed before plotting their data in Fig. 8, using their given instrumental resolution, an assumed Lorentzian profile of the zero slit width Raman line, and an assumed Gaussian instrument transmission function.

The variation with temperature in the FWHM for the synthetic-diamond–natural-diamond laminate is shown in Fig. 9. Also shown as a solid line is a third-order polynomial fit to the experimental data for natural diamond. The spectral lineshapes were again found to be well represented by a Voigt function and a similar technique was used to obtain the width of the Lorentzian component. The temperatures are obtained from the Stokes-to-anti-Stokes intensity ratio. The FWHM of the observed first-order Raman line in this synthetic-diamond–natural-diamond laminate is approximately 1 cm^{-1} greater than that for natural diamond, over the full observed temperature range. This difference between the natural and the synthetic-diamond–natural-diamond laminate FWHM is not as large as that found by other investigators [8], where widths several times greater are sometimes observed. This may be explained by the increased quality of the homoepitaxially grown diamond, but is also partly due to a superposition of the narrower Raman peak of the natural diamond substrate portion and the presumably wider Raman signal of the synthetic diamond portion of the diamond laminate. With modifications in the experimental set-up, it should be possible to distinguish between the two possibilities by collecting light from a very shallow depth of field that only encompasses one region of the material. Further improvements can be made by using near-resonance Raman scattering in the UV wavelength region. In this case, the laser will be attenuated within micrometers of the surface, making the characterization strategy near surface sensitive.

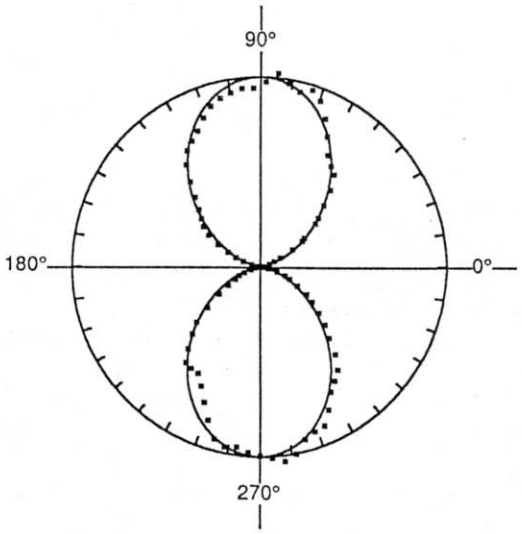

Fig. 10. Polar plot for the peak signal of the room temperature Stokes Raman spectra of the synthetic-diamond–natural-diamond laminate. The solid line is eqn. (1).

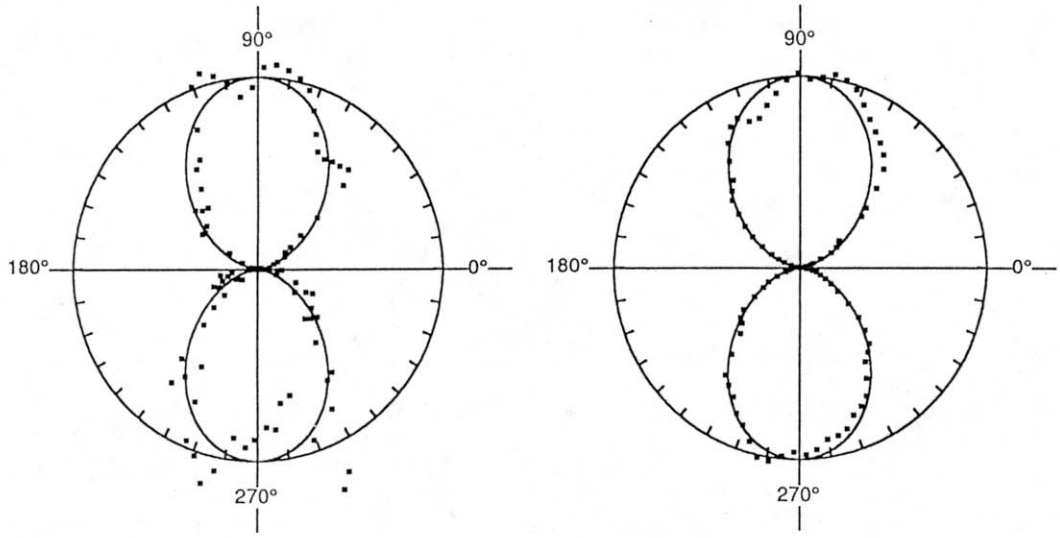

Fig. 11. Polar plots for the peak signal of the anti-Stokes (left graph) and the Stokes Raman spectra. The synthetic-diamond–natural-diamond laminate temperature was 600 K.

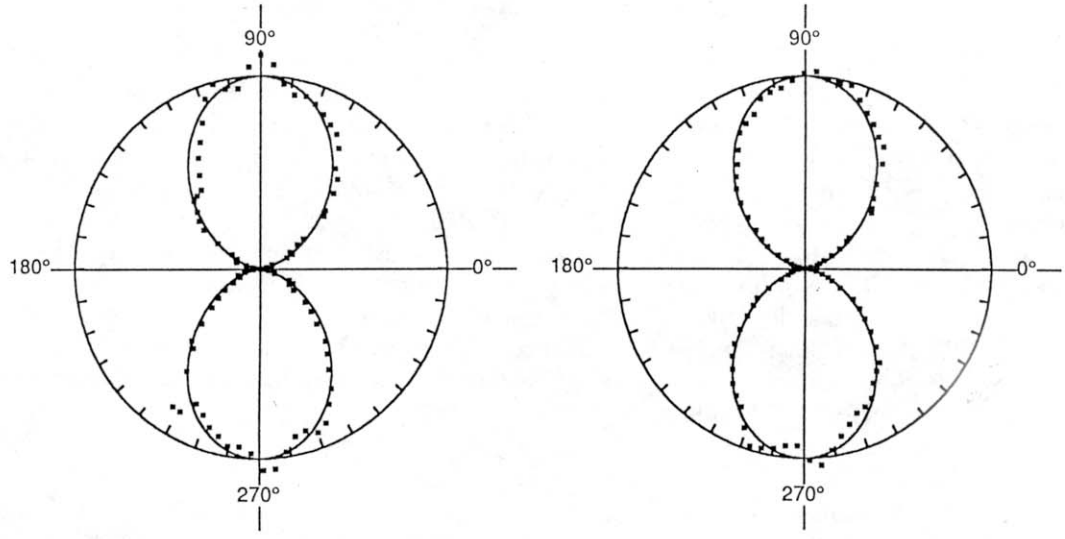

Fig. 12. Polar plots for the peak signal of the anti-Stokes (left graph) and the Stokes Raman spectra. The synthetic-diamond–natural-diamond laminate temperature was 1200 K.

3.3. First-order Raman polarization

At room temperature, the polarization of the Raman scattered light for the natural diamond samples with a (100) orientation was found to behave as predicted by eqns. (1) and (2). The light was linearly polarized with an angle that depended on the crystal rotation about the x axis. The Raman signal from natural diamond crystal samples with (111) orientation was separately found to have no linear polarization, again as expected. The homoepitaxially grown synthetic-diamond–natural-diamond laminate was also investigated for its polarization properties at room temperature and above, since it was grown on a (100) oriented single crystal. At all temperatures from 300 to 1200 K, no significant depolarization of the Raman signal was found. This is shown in Figs. 10–12, where polar plots for 300 K, 600 K, and 1200 K respectively are given. The anti-Stokes polar plots are only shown for 600 K and 1200 K owing to a rapidly decreasing signal to noise ratio at lower temperatures. In these diagrams, the magnitude of the distance from the origin represents the relative scattering intensity. The angle is measured from the principal y axis of the crystal. The peak levels have been normalized to unity. The solid line represents the predictions of eqn. 1. This behavior is a strong indication that the homoepitaxially grown diamond has retained the single-crystal structure. Furthermore, no significant difference is observed between the shape of

the room temperature and high temperature polar plots, suggesting that depolarization arising from two-phonon decay appears to be insignificant. The polycrystalline region immediately adjacent to the single-crystal region was also investigated. This region showed no evidence of linear polarization and hence no indication of single-crystal growth.

4. Conclusions

The variation with temperature of the first-order Stokes and anti-Stokes Raman signals for homoepitaxially grown synthetic-diamond – natural-diamond laminate have been presented. The Raman shift measurements indicate that, as grown, this sample is under some stress. We speculate that this stress is caused by hydrogen incorporation during growth. The Raman width measurements are less definitive but, being close to the width of natural diamond, are indicative of high quality deposition. It has also been shown through analysis of the polarization of the macro-Raman signal that the homoepitaxially grown diamond is a single crystal, and that the Raman signal that allows this determination is effective at high temperatures, including those at which CVD diamond is formed. Finally, an extension to 2000 K of the experimental results describing the temperature variation in the first-order Raman spectrum of natural type IIa diamond has been presented.

Acknowledgments

This work is supported in part by the Office of Naval Research. The loan of Nd/YLF laser to us by Spectra-Physics is gratefully acknowledged. Crystallume would like to acknowledge the support from SDIO/IST managed through the Office of Naval Research.

References

1 R. C. DeVries, *Annu. Rev. Mater. Sci.*, *17* (1987) 161.
2 J. C. Angus and C. C. Hayman, *Science*, *241* (1988) 913.
3 S. Matsumoto, Y. Sato, M. Tsutsumi and N. Setaka, *J. Mater. Sci.*, *17* (1982) 3106.
4 S. A. Grot, S. Lee, G. Sh. Gildenblat, C. W. Hatfield, C. R. Wronski, A. R. Badzian, T. Badzian and R. Messier, *J. Mater. Res.*, *5* (1990) 2497.
5 C. B. Zarowin, N. Venkataramanan and R. R. Poole, *Appl. Phys. Lett.*, *48* (1986) 759.
6 C. Herring, *Phys. Rev.*, *95* (1954) 954.
7 H. Boppart, J. van Straaten and I. F. Silvera, *Phys. Rev. B*, *32* (1985) 1423.
8 D. S. Knight and W. B. White, *J. Mater. Res.*, *4* (1989) 385.
9 P. Zorabedian and F. Adar, *Appl. Phys. Lett.*, *43* (1983) 177.
10 R. A. Cowley, *J. Phys.*, *26* (1965) 659.
11 C. Postmus and J. R. Ferraro, *Phys. Rev.*, *174* (1968) 983.
12 P. G. Klemens, *Phys. Rev.*, *148* (1966) 845.
13 R. G. N. Nayar, *Proc. Indian Acad. Sci. A*, *13* (1941) 284.
14 C. V. Raman, *Proc. Indian Acad. Sci. A*, *26* (1948) 339–355.
15 R. S. Krishnan, *Proc. Indian Acad. Sci. A*, *24* (1946) 45.
16 S. A. Solin and A. K. Ramdas, *Phys. Rev. B*, *1* (1970) 1687.
17 E. Anastassakis, H. C. Hwang and C. H. Perry, *Phys. Rev. B*, *4* (1971) 2493.
18 W. J. Borer, S. S. Mitra and K. V. Namjoshi, *Solid State Commun.*, *9* (1971) 1377.
19 H. Herchen and M. A. Cappelli, *Phys. Rev. B*, *43* (1991) 11740.
20 E. S. Zouboulis and M. Grimsditch, *Phys. Rev. B*, *43* (1991) 12490.
21 R. Loudon, *Adv. Phys.*, *13* (1964) 423.
22 M. Yoshikawa, H. Ishida, A. Ishitani, S. Koizumi and T. Inuzuka, *Appl. Phys. Lett.*, *58* (1991) 1387.
23 P. Brüesch, in P. Fulde (ed.), *Phonons: Theory and Experiments II*, Springer Series in Solid-State Sciences Vol. 65, Springer, New York, 1986, p. 99.
24 R. J. Nemanich, D. K. Biegelson, R. A. Street and L. E. Fennell, *Phys. Rev. B*, *29* (1984) 6005.
25 A. Compaan and H. J. Trodahl, *Phys. Rev. B*, *29* (1984) 793.
26 R. Tsu and G. Hernandez, *Appl. Phys. Lett.*, *41* (1982) 1016.
27 L. N. Latyev, V. Ya. Chekhovski and E. N. Shestakov, *High Temp. High Pressures*, *2* (1970) 175.
28 G. D. Kubiak, A. V. Hamza, R. H. Stulen, E. C. Sowa, K. W. Kolasinski, M. A. Van Hove, *Proc. Second Int. Conf. on New Diamond Science and Technology*, Materials Research Society, Pittsburgh, PA, 1990, p. 21.